Gaze Point Projection by Marker-Based Localization of Eye-Tracking Glasses for Examining Trust in Automated Vehicles

Franz Albers and Univ.-Prof. Dr.-Ing. Prof. h.c. Dr. h.c. Torsten Bertram
TU Dortmund University, Institute of Control Theory and Systems Engineering, 44227 Dortmund, Germany

Abstract

Human trust in automated systems is a major factor for the acceptance of automated vehicles. In this paper, an approach for marker-based visual localization of eye-tracking glasses in a vehicle is proposed. The estimated pose of the eye-tracking glasses within a 3D model of the vehicle is utilized to infer the 3D gaze point with respect to the vehicle frame by ray casting. The approach is utilized in a Wizard-of-Oz study on a test track to analyze the gaze behavior of drivers in terms of their trust in automated vehicles. Objective gaze-related measures are compared to subjective self-assessments of the participants. Results show, depending on the participant, more or less consistent objective and subjective assessments.

1 Motivation

Automated driving promises improved traffic safety and comfort for road users. While fully driverless vehicles according to SAE Level 5 are aspired for the future, necessary technologies and legislations are still under research and development. Recently, the first conditionally automated vehicles according to SAE Level 3 [1] were legally permitted and are scheduled for release in Germany[1]. Conditionally automated vehicles allow the user for the first time to engage in non-driving related tasks (NDRTs) while driving. However, whenever a system limit is reached, the user is expected to take over the driving task within a reasonable time. The sudden change of role from distracted passenger to attentive driver constitutes a challenging task for many users. Thus, driver monitoring systems are gaining importance and are becoming obligatory for new vehicles in the EU in 2022[2]. Being driven by an automated system can feel uncommon for many people, which makes trust in and acceptance of automated vehicles very important and major research topics.

Eye-tracking-based approaches are among the most promising driver monitoring methods since they provide good attention estimations for forward-looking drivers and non-intrusive external eye-tracking systems exist. However, external systems tend to fail whenever the driver turns his head (e.g. shoulder check) and eye-tracking glasses usually provide less missed and better accuracy for pupil-related measurements like the pupil diameter, which e.g. can be used to estimate the cognitive workload of a user with the Low/High Index of Pupillary Activity (LHIPA) [2]. Thus, the pupil diameter is an interesting indicator for researching the driver state. On the downside, portable eye-tracking systems are obtrusive and have no fixed coordinate frame with respect to the vehicle frame, which makes image processing a requirement for utilizing gaze tracking data in online applications (e.g., [3]).

Knowing the exact pose of the eye-tracking glasses is crucial for online processing of gaze data, e.g. for relating the eye-tracking data to the environmental model or for adapting the takeover request according to the driver's field of view to avoid any additional distractions. This paper proposes an approach for online visual localization of eye-tracking glasses within a driving simulator or test vehicle by exploiting fiducial markers that are either distributed over the screens of a driving simulator or both the exterior and interior of a test vehicle as landmarks. Some markers are also directly attached to the sensor housings, e.g. to the bottom of the lidar baseplate, in order to easily relate the pose of the eye-tracking glasses to the reference lidar frame. Each planar marker provides four correspondence points that can be used to accurately estimate the pose of the front-facing scene camera of the eye-tracking glasses.

A similar approach for marker-based localization of the eye-tracking glasses was proposed for examining traffic awareness of drivers [4]. In the paper at hand, we utilize the pose estimation of the eye-tracking glasses to process data recorded in a Wizard-of-Oz study. Furthermore, we compare the observations with subjective self-assessments of the participants to analyze their trust in automated vehicles.

2 Gaze Point Projection

In this section, the proposed method for projecting the gaze point estimated by the eye-tracking glasses (*Tobii Pro Glasses 2*) into the lidar reference coordinate system is described in detail. First, the eye-tracking glasses are localized in a prerecorded 3D marker map by estimating the scene camera pose from planar fiducial ArUco markers (section 2.1). The estimated pose of the eye-tracking glasses is tracked with a Kalman Filter (section 2.2) and used as the

[1] https://www.adac.de/rund-ums-fahrzeug/ausstattung-technik-zubehoer/autonomes-fahren/technik-vernetzung/autonomes-fahren-staupilot-s-klasse/

[2] https://www.bmvi.de/SharedDocs/EN/Articles/StV/Roadtraffic/new-vehicle-safety-systems.html

ISBN 978-3-8007-6113-5

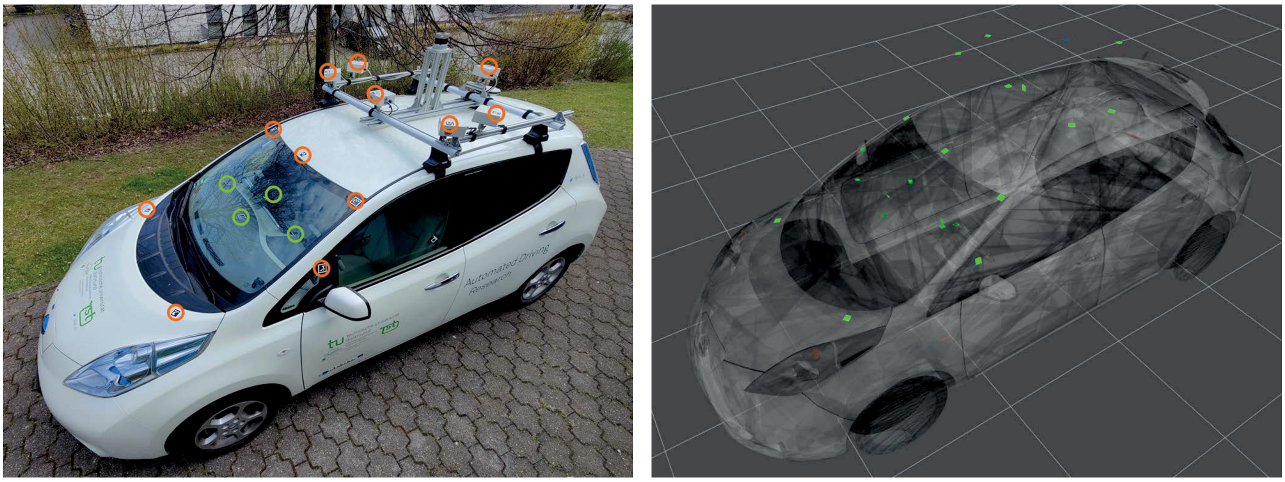

(a) Markers attached to the interior (circled green) and exterior (circled orange) of the test vehicle. Further markers are attached to the bottom of the lidar baseplate, behind the front camera and in the interior.

(b) Virtual marker map with markers attached to both the interior and exterior of the vehicle displayed in rviz. The blue marker represents the marker attached to the bottom of the lidar baseplate.

Figure 1 Visualization of real and virtual marker maps of the test vehicle. Note, some of the markers visible in the transparent virtual visualization are concealed in the photo of the test vehicle.

origin of the gaze. The gaze is related to the environment by casting (gaze) rays from the tracked scene camera pose to the estimated 3D gaze point in a 3D occupancy grid model of the test vehicle (section 2.3).

2.1 Marker-Based Localization

ArUco markers are commonly used as landmarks in robotic applications since they are computationally effectively detectable in camera images ([7]). Multiple ArUco markers with different IDs are adhered to both the interior and the exterior of the test vehicle as shown in figure 1a. The markers inside the vehicle are mainly distributed around the co-driver's seat, which is the participant's seat in the Wizard-of-Oz study (see section 3). For transforming the estimated pose from the *markermap* frame to the reference *lidar* frame (and hence, the vehicle frame transformation tree), the origin marker of the marker map is attached to the bottom of the lidar baseplate. The lidar frame is located on the bottom center of its housing. Thus, the transformation between both frames is simply described by a 2 cm offset (equal to the baseplate thickness) in the z-direction and a roll angle of 180°, because the marker is fixed upside-down. Further markers are distributed over the vehicle exterior and the camera sensors on the rooftop for creating a closed pose graph from the origin marker below the lidar to the markers inside the vehicle.

A reference map of the attached markers is created from an optimized pose graph using the ArUco library [6] prior to the experiment. The resulting marker map in conjunction with a semi-transparent CAD mesh model of the test vehicle is displayed in figure 1b.

Markers are observed continuously by the scene camera of the eye-tracking glasses with a frame rate of 25 Hz and detected with the ArUco library ([5]). By recognizing poses and IDs of detected markers, the pose of the front-facing scene camera of the eye-tracking glasses is estimated.

2.2 Scene Camera Pose Tracking

Due to outliers and possibly no detected markers in some frames (and hence no new measurements for the scene camera pose), the estimated scene camera pose is filtered using a linear Kalman filter for position and orientation tracking according to [8]. The state vector $\mathbf{x}$ is composed of the translation x, y and z and roll, pitch and yaw angles ψ, θ and ϕ for rotation of the scene camera with respect to the *markermap* frame as well as their first and second derivatives:

$$\mathbf{x} = (x, y, z, \dot{x}, \dot{y}, \dot{z}, \ddot{x}, \ddot{y}, \ddot{z}, \psi, \theta, \phi, \dot{\psi}, \dot{\theta}, \dot{\phi}, \ddot{\psi}, \ddot{\theta}, \ddot{\phi})^T \tag{1}$$

The process model relates the state $\mathbf{x}_k$ with the previous state $\mathbf{x}_{k-1}$ and the previous normal distributed process noise $\mathbf{w}_{k-1}$:

$$\mathbf{x}_k = \begin{pmatrix} A_T & \mathbf{0} \\ \mathbf{0} & A_T \end{pmatrix} \mathbf{x}_{k-1} + \mathbf{w}_{k-1} \tag{2}$$

Matrix A_T in the previous equation is defined with the inter frame arrival time $\Delta t = 1/r_{\text{fps}}$ (with r_{fps} being the frame rate) as follows:

$$A_T = \begin{pmatrix} I & \Delta t I & \frac{1}{2}(\Delta t)^2 I \\ \mathbf{0} & I & \Delta t I \\ \mathbf{0} & \mathbf{0} & I \end{pmatrix} \tag{3}$$

I is defined here as the 3×3 identity matrix. The measurement model defines the measured pose variables x_k, y_k, z_k, ψ_k, θ_k and ϕ_k:

$$\mathbf{p}_k = \begin{pmatrix} x_k \\ y_k \\ z_k \\ \psi_k \\ \theta_k \\ \phi_k \end{pmatrix} = \begin{pmatrix} I & \mathbf{0} & \mathbf{0} & \mathbf{0} & \mathbf{0} & \mathbf{0} \\ \mathbf{0} & \mathbf{0} & \mathbf{0} & I & \mathbf{0} & \mathbf{0} \end{pmatrix} \mathbf{x}_k + \mathbf{v}_k \tag{4}$$

ISBN 978-3-8007-6113-5

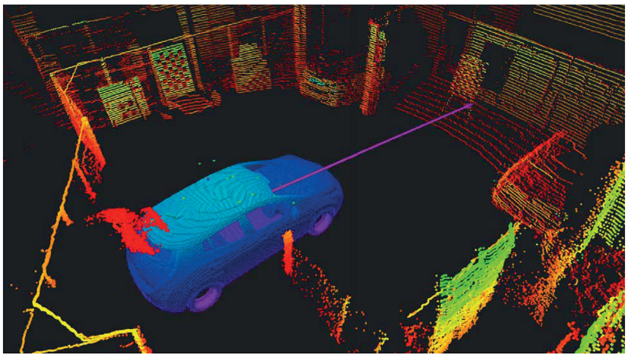

(a) The 3D occupancy grid of the vehicle model (in blue) and the casted gaze ray from the filtered scene camera pose to the estimated 3D gaze point (purple).

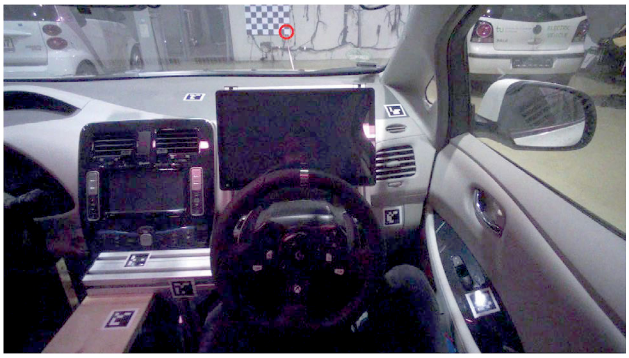

(b) Corresponding gaze point visualized as red circle in the eye-tracking scene camera image

Figure 2 Comparison of the estimated 3D gaze point and the 2D gaze point recorded by the eye-tracking glasses

Whenever the pose $\mathbf{p}_k$ could not be estimated in a frame due to undetected markers, the estimated pose is set to the previous estimation ($\mathbf{p}_k = \mathbf{p}_{k-1}$) and the measurement noise covariance $\mathbf{v}_k$ is increased until a limit is reached.

Fusing additional measurements (e.g., ego-vehicle motion-compensated measurements of the built-in gyroscope and accelerometer of the glasses or the head pose estimated by face tracking algorithms like OpenFace [9]) for more precise pose estimation of the eye-tracking glasses, especially in the case of undetected markers, promises enhanced results, but was not conducted in this research.

2.3 Gaze Ray Casting in a 3D Occupancy Grid

With the filtered pose of the scene camera being utilized as the origin for the gaze tracking data, the 3D gaze point estimated by the eye-tracking glasses can be matched to a model of the vehicle or to the environment model. In this work, a CAD model of the test vehicle is converted to a 3D occupancy grid. The 3D occupancy grid is used to distinguish between attentive gazes to the road and distracted gazes to the interior of the vehicle by ray casting (see figure 2). The *octomap* library [10] is utilized for efficiently computing intersections with the 3D occupancy grid.

Humans are capable of perceiving not only the gaze point but also a certain field of view with peripheral vision. The visual field from which information is perceivable with a single gaze and without any further eye movements is called the useful field of view [11]. Dependent on the individual, a non-linear drop in performance was observed at around 20° to 30° measured from the optical axis of the eyes [12]. Degradation of the useful field of view was observed for aging persons [13]. Building upon these results, a useful visual field of $\alpha = 20°$ measured from the optical axis of the eyes is assumed in this work.

To account for the useful field of view of the driver, multiple rays are cast within a cone with an aperture of 2α. The apex of this cone lies in the filtered scene cam origin and the axis of the cone is equal to the gaze ray. In case the eye-tracking glasses are localized within the vehicle and all of these rays are hitting the vehicle model occupancy grid, the participant is classified as distracted. Otherwise, the participant/driver is expected to be looking towards the road.

2.4 Results: Gaze Point Projection

A comparison of an estimated 3D gaze point and the high precision 360° lidar of the test vehicle with the corresponding original gaze point in the scene camera image of the eye-tracking glasses in a test setup is provided in figure 2. The participant gazed at the lower right-hand corner of the checkerboard for several seconds (see figure 2b), which is accurately resembled in the 3D *lidar* frame 2a.

Obviously, the accuracy of the projected gaze point strongly depends on the accuracy of the localization of the eye-tracking glasses within the vehicle, which in turn depends on the number of detected markers. Due to missing ground truth measurements for the eye-tracking glasses' pose, the 3D gaze point projection is evaluated only visually. Throughout the recording, the accuracy of the gaze estimation was observed to be below 2°, which is slightly above the accuracy reported by the manufacturer[3]. Whenever the Tobii Glasses are well localized, deviations in the 3D gaze point coincided with the 2D gaze point, which results in an accuracy below 2°.

The pose estimation of the eye-tracking glasses runs in real-time with 25 Hz. Gaze data is evaluated at 100 Hz.

3 Wizard-of-Oz Human Subject Study

The presented approach is applied in a human subject study (17 participants, 10 male, and 7 female, mean age 26.9 years, ranging from 23 years to 41 years with a standard deviation of 4.28 years). Data from one participant was disregarded due to technical issues.

Participants were fooled into thinking they were driven automatically and occasionally required to take over the

[3] Tobii Pro Glasses 2 Quality Report - Accuracy, precision and detected gaze under optimal conditions in a controlled environment (https://www.tobiipro.com/siteassets/tobii-pro/accuracy-and-precision-tests/tobii-pro-glasses-2-accuracy-and-precision-test-report.pdf)

driving task upon request, though a hidden safety driver was operating the test vehicle during the whole experiment [14]. This setup is known as Wizard-of-Oz vehicle and is described in detail in section 3.1. Wizard-of-Oz vehicles are commonly used in human-factors research to prototype automated vehicles while they are not commercially available as a more realistic alternative to (static) driving simulators.
The study was conducted in summer 2020 on a test track and is described in detail in [14]. The data was recorded in the *rosbag* format[4] and utilized for this work later.

3.1 Wizard-of-Oz Vehicle

The test vehicle (see figure 1a) is equipped with a lidar sensor (*Ouster OS1*) and several cameras for perceiving the environment (six *FLIR Chameleon 3* for a 360° view, one front-facing *Mobileye 630*) and a RTK-DGPS (*GeneSys ADMA-G*). Internal CAN messages (e.g., velocity or steering angle) of the vehicle are logged. For monitoring the participant, eye-tracking glasses are utilized with the *Tobii-GlassesPyController* [15]. Additionally, two interior RGB-D cameras (*Intel RealSense D435*) for monitoring the participant are installed and an *Empatica E4* bracelet is used for capturing physiological data. As an underlying communication framework, the Robot Operating System (ROS) is utilized for capturing data of all sensors synchronously.

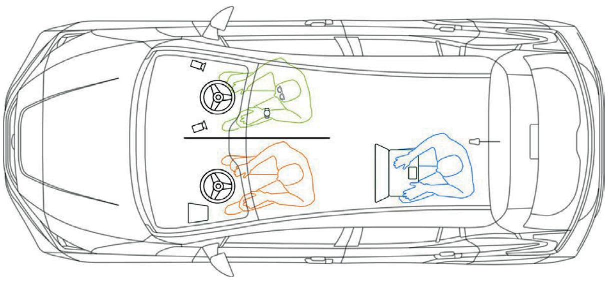

Figure 3 Wizard-of-Oz experiment setup (borrowed from [14], adapted from [16])

The Wizard-of-Oz vehicle is built up similarly to the RRADS platform [14, 16]. Two persons are in charge of the experiment: The *Driving Wizard* (depicted orange in Figure 3), who operates the vehicle during the whole experiment, and the *Interaction Wizard* (blue), who sits on the rear seat and serves as experiment supervisor and contact person for the participant. The test vehicle is equipped with a second steering wheel and pedals on the co-driver's seat, which is where the participant (green) sits during the trial. Thus, the participant is under the impression of sitting in a right-hand drive vehicle. A divider wall is installed between both front seats, which is designed in a way that both the *Driving Wizard* and the participant can see the complete windshield but not each other.
The participant is instructed that even though a safety driver sits on the driver's seat, it is rather a safety requirement due to the experimental state of the system and that the safety driver would intervene only in case of serious system malfunctions while the vehicle drives automatically on the test track. This leaves the participant under the impression of being driven automatically, while in fact, the *Driving Wizard* is operating the vehicle at all times. This illusion is supported by the sensor suite on top of the vehicle and the technical devices in the trunk. The second steering wheel is actuated to follow the original steering wheel angle in real-time using data decoded from the vehicle CAN bus. Likewise, indicator light and speed signals are decoded from the CAN bus and displayed on the participant's instrument cluster.
As an extension of the RRADS platform, the Wizard-of-Oz vehicle enables the simulation of a temporary takeover of the driving task by the test person. In case a takeover request is issued, the subject can either take over the driving task by pressing the button for automated driving functions on the steering wheel, the brake or accelerator pedal, or by a steering intervention, which is detected by a steering wheel angle observer. The commands issued by the test person are displayed to the *Driving Wizard* on a small graphical user interface in his field of view. This enables him to resemble the vehicle control commands of the test person. A realistic experience requires almost instant reactions of the Driving Wizard, which were minimized by practice and a predefined route on the test track.
Results showed that most participants subjectively experienced the Wizard-of-Oz experiment as realistic or very realistic automated drive [14].

3.2 Test Procedure

The experiment was conducted on a dedicated test track[5]) and was approved by the ethics committee of the TU Dortmund University beforehand.
Prior to each road test, participants were instructed regarding gathered sensor data and personal data and about the general test process. After consent, each participant completed a questionnaire regarding their usual driving habits and their attitude towards automated vehicles [17]. The participants received a short introduction of the functionality of the test vehicle (e.g., sensors, dashboard, occasional visual and auditory takeover requests). They also were equipped with a physio bracelet and eye-tracking glasses, which were calibrated at the start of the experiment.
The *Driving Wizard* operated the vehicle during the course of the experiment to fool the participant into thinking the vehicle was driving automatically. A speed delimiter at $30\,\mathrm{km\,h^{-1}}$ was active throughout the whole experiment. During the total driving duration of nearly 30 minutes, four takeover requests were issued. The first of these was performed for familiarization purposes.
Throughout the experiment, participants were asked at specific times to either perform a NDRT or to monitor the automated vehicle attentively. The tablet game *Subway Surfers* served as a NDRT in this experiment. Each participant completed two NDRTs for a time period of two to six minutes per activity.
After the road trial, participants filled out a second questionnaire for evaluating the overall driving experience and the trust they had in the automated vehicle.

[4] *rosbag documentation* (http://wiki.ros.org/rosbag)

[5] LaSiSe Test Track https://www.lasise.de/ueber-uns/Testgelaende/

Table 1 Results of the Wizard-of-Oz experiment. On the left side, the table shows for each participant the total time of observed NDRTs, the percentage of time for which marker-based pose estimation for the eye-tracking glasses was possible, the number, frequency and mean duration of gazes to road. On the right side, corresponding questionnaire answers on a 5-Level Likert scale (Strongly disagree (1), Disagree (2), Neither agree nor disagree (3), Agree (4), Strongly agree (5)) to the items "Self-driving vehicles will be safe" (Q1), "Self-driving vehicles will be reliable" (Q2), "One should be suspicious towards self-driving vehicles" (Q3) and "Recalling the self-driving ride, I trusted the system" (Q4) are displayed. Note the reversed coding of Item Q3 for checking consistency of answers. Q1, Q2 and Q3 are answered prior to the driving experiment, Q4 is answered retrospectively.

	Objective Measures					**Subjective Measures**			
Subject	Total NDRT Time [s]	Ratio of Poses estimated [%]	No. of Gazes to Road [1]	On-Road Gaze Freq. [Hz]	Mean Gaze Duration [s]	Q1	Q2	Q3	Q4
1	377.97	94.25	12	0.03	1.06	-	-	-	-
2	75.26	79.63	2	0.03	0.43	3	2	2	4
3	371.82	78.15	0	0.00	-	4	4	1	5
4	377.88	66.39	22	0.06	1.90	4	4	3	4
5	537.48	63.92	25	0.05	0.94	4	4	3	5
6	573.62	82.55	34	0.06	0.70	3	3	1	5
7	557.88	93.27	31	0.06	0.82	5	4	2	5
8	373.58	59.08	2	0.01	0.24	5	4	5	5
9	555.68	68.61	40	0.07	0.81	4	4	2	4
10	374.22	18.51	1	0.00	0.38	3	3	3	5
11	447.34	94.80	49	0.11	0.61	5	5	2	5
12	455.65	2.34	60	0.13	0.69	4	4	2	4
13	494.20	93.19	52	0.11	0.60	3	3	4	3
14	369.57	87.78	12	0.03	1.21	4	3	3	4
15	682.47	86.21	86	0.13	0.88	4	4	2	4
16	546.03	81.08	42	0.08	0.51	4	4	3	1

3.3 Objective Results: Wizard-of-Oz Study

Table 1 depicts the results of the presented approach being applied to the previously recorded data of the Wizard-of-Oz study. Results were sanity checked by viewing the corresponding gaze tracking video stream. For each participant, the recorded data comprised approx. 6 and 12 minutes of NDRTs, except for participant 2, who ended both NDRTs early due to motion sickness.

The ratio of estimated poses (see Table 1) depends on the detected fiducial markers in the scene camera image and strongly varies across participants. While for most participants the scene camera pose was estimated for a big majority and for some participants even for more than 90 % of frames, only very few pose estimations were possible on the data recorded from participants 10 and 12. These participants used to sit or to hold the tablet in a way where necessary markers were concealed.

Estimated gazes to the road were disregarded, if the duration was shorter than 100 ms. Multiple gazes to the road were considered as a single gaze to the road if they were less than 500 ms apart.

Large variations between individuals were also observed for the on-road gaze frequency. Whereas some participants (especially 11, 12, 13, 15) looked up every few seconds to check the traffic situation, participants 1,2,3,8, and 10 were completely engaged in the NDRT and seemed to fully trust the automated system right from the start. Both observations could also be artifacts due to being driven automatically within a research study: Attentively looking participants might have expected a takeover situation, while completely engaged participants might have trusted the additional safety driver rather than the automated system.

The on-road gaze frequency apparently correlates with the mean gaze duration: While participants 1, 4, 5, 14 checked the road for rather long durations, but more seldomly, participants checking the road frequently usually gazed shorter. Most participants that were completely engaged in the NDRT (2, 8, 10) also exhibited the fastest gazes to the road.

3.4 Comparison with Self-Assessment

Table 1 shows on the right-hand side the results of the questionnaire for the scale trust in automated vehicles [17]. Items Q1 to Q4 are explained in the table description. Items Q1 to Q3 indicate the general trust in automated vehicles. Overall, participants have a rather positive opinion of automated vehicles. Participants 2, 6, 10, 13 seem to exhibit the least trust in automated vehicles, as can be concluded from the negative and neutral answers for Q1 and Q2 and positive answers for Q3 (reversed coding). Out of these, three participants retrospectively answered that they trusted the automated system of the test vehicle (Q4), which they also showed with their gaze behavior: Participants 2 and 10 barely looked up from their NDRTs at all. Note, that participant 10 also had a very low ratio of estimated poses. However, the result was visually confirmed. Participant 6 showed medium on-road gaze frequencies and gaze durations. Participant 13, however, was among the most atten-

tive drivers and frequently checked the traffic situation.
Participant 12, who was among the most attentive drivers and confirmed his trust in the automated system retrospectively, commented after the ride that "It will take many [automated] rides until you actually trust the system and engage in other things while sitting on the driver's seat."

4 Conclusion

This paper presented an approach for marker-based localization of eye-tracking glasses in a vehicle. The approach was used to compare the gaze behavior of drivers and their self-assessments of trust in automated vehicles within a Wizard-of-Oz human subject study. Results indicated large differences in the gaze behavior during NDRTs. However, the group of participants was too small to draw absolute conclusions between the gaze behavior and trust.
The proposed approach for estimating the attention of the driver constitutes a rather simple application demonstrating the use of the eye-tracking glasses' pose within the vehicle. Further applications and extensions are possible. E.g., the exact gaze point within the vehicle can be utilized online to offer supporting stimuli for the driver, e.g. by issuing an adaptive visual takeover request directly in the field of view of the driver. The pose could also be used to relate the driver's gaze to the environmental model in order to support the driver in anticipation of possibly overseen road users. The approach can easily be adapted to different environments. E.g., by utilizing the 3D gaze point in a static driving simulator, scenarios can be triggered depending on the gaze point. Due to the intrusive nature of eye-tracking glasses, this approach is intended to be used in research.

Acknowledgement

The authors would like to thank Julian Golembiewski, Sergej Stepcenkov, Daryna Sytnychenko, and Mohamad Hani Slim for contributing to this work.

Funding

This work was funded by German Federal Ministry of Transport and Digital Infrastructure (research project "MoFFa", grant number 16AVF2005) and by the District Council Arnsberg (research project "DEmandäR").

5 Literature

[1] SAE International: *Taxonomy and Definitions for Terms Related to Driving Automation Systems for On-Road Motor Vehicles (J3016)*. 2. Ed. SAE International, 2018

[2] Duchowski, A. T., Krejtz, K., Gehrer, N. A., Bafna, T., Bækgaard, P.: *The low/high index of pupillary activity*. Proceedings of the 2020 CHI Conference on Human Factors in Computing Systems, 2020, pp. 1-12

[3] Hugenroth, A., Albers, F., Oeljeklaus, M., Bertram, T.: *Object Classification in the Fixation of a Car Driver*. AmE 2020 - Automotive meets Electronics; 11th GMM-Symposium, 2020, pp. 1-6.

[4] Langner, T., Seifert, D., Fischer, B., Goehring, D., Ganjineh, T., Rojas, R.: *Traffic awareness driver assistance based on stereovision, eye-tracking, and head-up display*. IEEE International Conference on Robotics and Automation (ICRA), 2016, pp. 3167–3173

[5] Garrido-Jurado, S., Muñoz Salinas, R., Madrid-Cuevas, F.J., Medina-Carnicer, R.: *Generation of fiducial marker dictionaries using mixed integer linear programming*. Pattern Recognition, 51, pp. 481-491, 2016

[6] Muñoz-Salinas, R., Marín-Jimenez, M. J., Yeguas-Bolivar, E., Medina-Carnicer, R.: *Mapping and localization from planar markers*. Pattern Recognition, 73, 2018, pp. 158-171

[7] Romero-Ramirez, F.J., Muñoz-Salinas, R. Medina-Carnicer, R.: *Speeded up detection of squared fiducial markers*. Image and Vision Computing, vol 76, 2018, pp. 38-47

[8] Pentenrieder, K. (2005). *Sensor Fusion using the Kalman Filter* [online]. http://campar.in.tum.de/Chair/KalmanFilter. Last checked: 12.01.2022.

[9] Baltrusaitis, T., Zadeh, A., Lim, Y. C., & Morency, L. P.: *Openface 2.0: Facial behavior analysis toolkit*. 13th IEEE international conference on automatic face & gesture recognition, 2018, pp. 59-66

[10] Hornung, A., Wurm, K.M., Bennewitz, M., Stachniss, C., Burgard, W.: *OctoMap: An Efficient Probabilistic 3D Mapping Framework Based on Octrees*. Autonomous Robots, vol 34, 2013, pp. 189-206

[11] Ball, K. K., Wadley, V. G., Edwards, J. D.: *Advances in Technology Used to Assess and Retrain Older Drivers*. Gerontechnology, 1(4), 2002

[12] Sanders, A. F.: *Some Aspects of the Selective Process in the Functional Visual Field*. Ergonomics, 13(1), 1970, pp. 101–117

[13] Schieber F., Gilland J.: *Age Differences in the Useful Field of View during Real-World Driving*. Proceedings of the Human Factors and Ergonomics Society Annual Meeting. 49(2), 2005, pp. 182-185.

[14] Albers, F., Dargahi Nobari, K., Braun, J., Bartsch, K., Bertram, T.: *Koordination von Übernahmemanövern beim hochautomatisierten Fahren unter Berücksichtigung der Fahrerverfügbarkeit*. Forschung im Ingenieurwesen, https://rdcu.be/cFrNA, 2021

[15] de Tommaso, D.; Wykowska, A.: *TobiiGlassesPySuite: An Open-source Suite for Using the Tobii Pro Glasses 2 in Eye-tracking Studies*. Proceedings of the 11th ACM Symposium on Eye Tracking Research & Applications (ETRA19), 46, 2019, pp. 1-5

[16] Baltodano, S., Sibi, S., Martelaro, N. Gowda, N. Ju, W.: *The RRADS platform: a real road autonomous driving simulator*. Proceedings of the 7th International Conference on Automotive User Interfaces and Interactive Vehicular Applications. ACM, 2015, pp. 281–288

[17] Schlüter, J., Hellmann, M., Weyer, J.: *Identifikation von Fahrertypen im Kontext des automatisierten Fahrens*. Forschung im Ingenieurwesen, 85 (4), 2021, pp. 945–955